

A New Highly Anisotropic Rh-Based Heusler Compound for Magnetic Recording

Yangkun He,* Gerhard H. Fecher,* Chenguang Fu, Yu Pan, Kaustuv Manna, Johannes Kroder, Ajay Jha, Xiao Wang, Zhiwei Hu, Stefano Agrestini, Javier Herrero-Martín, Manuel Valvidares, Yurii Skourski, Walter Schnelle, Plamen Stamenov, Horst Borrmann, Liu Hao Tjeng, Rudolf Schaefer, Stuart S. P. Parkin, John Michael D. Coey, and Claudia Felser

The development of high-density magnetic recording media is limited by superparamagnetism in very small ferromagnetic crystals. Hard magnetic materials with strong perpendicular anisotropy offer stability and high recording density. To overcome the difficulty of writing media with a large coercivity, heat-assisted magnetic recording was developed, rapidly heating the media to the Curie temperature T_c before writing, followed by rapid cooling. Requirements are a suitable T_c , coupled with anisotropic thermal conductivity and hard magnetic properties. Here, Rh_2CoSb is introduced as a new hard magnet with potential for thin-film magnetic recording. A magnetocrystalline anisotropy of 3.6 MJ m^{-3} is combined with a saturation magnetization of $\mu_0 M_s = 0.52 \text{ T}$ at 2 K (2.2 MJ m^{-3} and 0.44 T at room temperature). The magnetic hardness parameter of 3.7 at room temperature is the highest observed for any rare-earth-free hard magnet. The anisotropy is related to an unquenched orbital moment of $0.42 \mu_B$ on Co, which is hybridized with neighboring Rh atoms with a large spin-orbit interaction. Moreover, the pronounced temperature dependence of the anisotropy that follows from its T_c of 450 K , together with a thermal conductivity of $20 \text{ W m}^{-1} \text{ K}^{-1}$, make Rh_2CoSb a candidate for the development of heat-assisted writing with a recording density in excess of 10 Tb in.^{-2} .

The pace of doubling of information density on magnetic recording media has slackened in recent years, as the effective size of the perpendicularly recorded grains approached the superparamagnetic blocking diameter, which is the lower size limit for stable ferromagnetism, directly related to the magnetocrystalline anisotropy energy K_1 . To resist demagnetization by random thermal fluctuations, the volume V of a magnetic material must satisfy the empirical condition that $K_1 V / k_B T > 60$ ($K_1 V > 1.5 \text{ eV}$), where k_B and T are the Boltzmann constant and ambient temperature, respectively.^[1–3] For high-density magnetic recording media, strong perpendicular uniaxial anisotropy is required. To create a film for magnetic recording or a permanent magnet that remains fully magnetized regardless of its shape, K_1 should exceed $\mu_0 M_s^2$, where M_s is the spontaneous saturation magnetization. Therefore, the magnetic hardness parameter $\kappa = \sqrt{K_1 / (\mu_0 M_s^2)}$, a convenient figure of merit for permanent magnets,^[4] should be larger than 1. This is difficult to achieve

Dr. Y. He, Dr. G. H. Fecher, Dr. C. Fu, Dr. Y. Pan, Dr. K. Manna, Dr. J. Kroder, Dr. X. Wang, Dr. Z. Hu, Dr. W. Schnelle, Dr. H. Borrmann, Prof. L. H. Tjeng, Prof. C. Felser
Max-Planck-Institute for Chemical Physics of Solids
Dresden D-01187, Germany
E-mail: yangkun.he@cpfs.mpg.de; Gerhard.Fecher@cpfs.mpg.de
A. Jha, Prof. P. Stamenov, Prof. J. M. D. Coey
School of Physics
Trinity College
Dublin 2, Ireland

Dr. S. Agrestini
Diamond Light Source
Harwell Science and Innovation Campus
Didcot OX11 0DE, UK


Dr. J. Herrero-Martín, Dr. M. Valvidares
ALBA Synchrotron Light Source
Cerdanyola del Valles, Barcelona, Catalonia 08290, Spain

Dr. Y. Skourski
Dresden High Magnetic Field Laboratory (HLD-EMFL)
Helmholtz-zentrum Dresden-Rossendorf
Dresden 01328, Germany

Prof. R. Schaefer
Leibniz Institute for Solid State and Materials Research (IFW) Dresden
Helmholtz strasse 20, Dresden D-01069, Germany

Prof. R. Schaefer
Institute for Materials Science
TU Dresden, Dresden D-01062, Germany

Prof. S. S. P. Parkin
Max Planck Institute of Microstructure Physics
Halle 06120, Germany

 The ORCID identification number(s) for the author(s) of this article can be found under <https://doi.org/10.1002/adma.202004331>.

© 2020 The Authors. Published by Wiley-VCH GmbH. This is an open access article under the terms of the Creative Commons Attribution License, which permits use, distribution and reproduction in any medium, provided the original work is properly cited.

DOI: 10.1002/adma.202004331

in rare-earth-free materials, other than CoPt or FePt with the $L1_0$ structure.

The development of modern magnetic recording media spanned three generations. The first generation for tapes and disks depended on the shape anisotropy of acicular fine particles of ferrimagnetic or ferromagnetic oxides, $\gamma\text{Fe}_2\text{O}_3$ or CrO_2 ,^[5] which were magnetized in-plane. The second generation was based on hexagonal Co–Cr–Pt thin films with perpendicular magnetization, which is currently used in hard disks.^[6] But Cr decreases the K_1 of the Co–Pt alloy, limiting the recording density. An ideal material for recording should be hard for storage and soft for writing, because of the limited fields that can be generated by the miniature writing electromagnet. $L1_0$ FePt, a hard magnet with $K_1 = 6.6 \text{ MJ m}^{-3}$ and $\kappa = 2.02$, is the basis of new, third generation of heat-assisted magnetic recording (HAMR) media,^[7,8] where writing is realized by heating the material close to its Curie point with a laser-powered near-field transducer.^[9] However, its high T_c of 750 K makes rapid heating and cooling problematic as it takes time.^[10] To achieve a large temperature variation in K_1 , 10% Cu is doped to obtain a 100 K reduction in T_c , but this is accompanied by a big drop of K_1 to 0.8 MJ m^{-3} .^[3,11] Additionally, unavoidable disordered A1 FePt impurities with a smaller K_1 and a lower T_c make the stabilization of its properties difficult.^[12] Therefore, it is useful to look for new materials with a strong K_1 , a suitable T_c and good thermal conductivity for development as new thin-film media.

To achieve sufficient anisotropy, a noncubic crystal structure (e.g., tetragonal or hexagonal) and a large spin–orbit interaction with the right sign are needed. When looking for new materials with uniaxial magnetocrystalline anisotropy, a significant deviation of the c/a ratio from 1 for tetragonal or $\sqrt{8/3}$ for hexag-

onal structures, is sought. Moreover, it is important to pair a 3d metal (Mn, Fe, Co) that provides a substantial magnetic moment with a heavy atom that enhances the spin–orbit interaction. Rh is a 4d element where the spin–orbit interaction is larger than in 3d elements, and it acquires a small induced magnetic moment when paired with a 3d metal. Therefore, it is worthwhile looking for new opportunities in magnetic recording among Rh-based alloys with a tetragonal or hexagonal structure.

Heusler alloys are a large family of compounds with formula X_2YZ , where X and Y are usually transition metals and Z is a main group element.^[13,14] The abundant choice of elements provides great scope to search for new materials with specific properties. Rh_2CoSb has a $c/\sqrt{2}a$ ratio of 1.24, the largest among all reported Rh-based magnetic Heusler compounds ($c/\sqrt{2}a$ is used to describe the tetragonal distortion relative to a cubic lattice). A magnetic moment per formula of $1.4 \mu_B$ in an 0.7 T applied field and a T_c of about 450 K were reported for polycrystalline samples many years ago.^[15] Recent ab initio calculations proposed uniaxial anisotropy with an easy c -axis.^[16] Both experiments and calculations suggest that Rh_2CoSb might be an interesting hard magnetic material.

Here, we study the anisotropic magnetic, thermal, and transport properties, as well as the temperature-dependent anisotropy of single crystals of Rh_2CoSb and investigate the contribution of rhodium to the magnetism.

Magnetic Heusler alloys with a tetragonal structure are often Mn-based with space group $I4m2$.^[17–22] However, the Mn–Mn magnetic coupling is usually antiferromagnetic at the nearest-neighbor separation in this structure, leading to ferrimagnetic order with relatively low magnetization (Figure 1a). Some tetragonal Rh-based Heusler alloys including

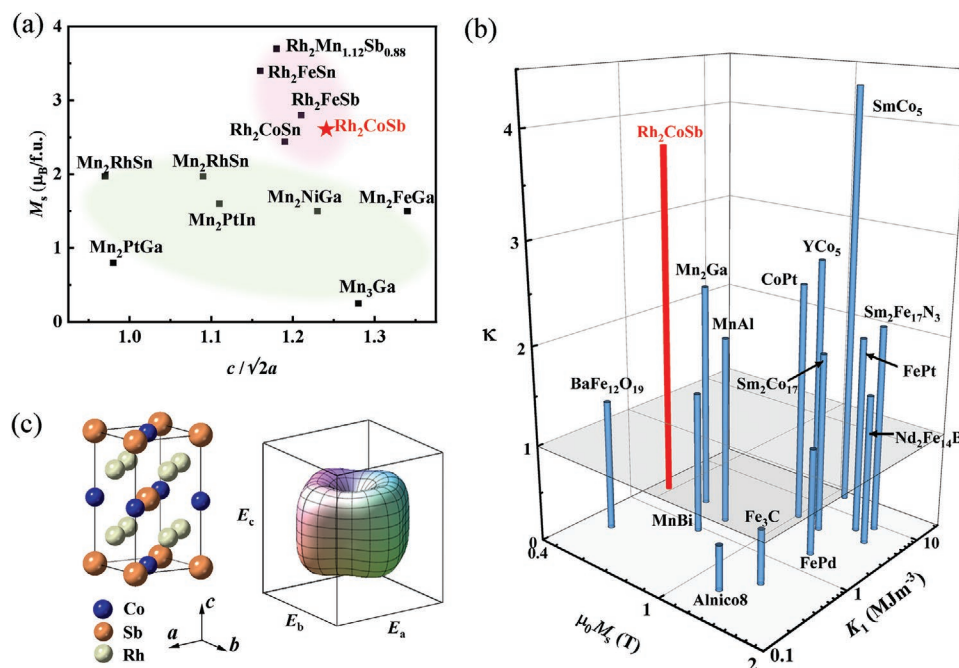


Figure 1. Tetragonal structure of Rh_2CoSb . a) Tetragonal distortion versus magnetic moment for Mn-based and Rh-based Heusler compounds. Rh-based compounds show both large distortion and large magnetization. Note that some compounds do not saturate in the applied magnetic fields of 7 T for Mn_2PtGa , 10 T for Mn_2FeGa , 6.6 T for Rh_2CoSn and Rh_2FeSn , and 0.7 T for Rh_2FeSb and $\text{Rh}_2\text{Mn}_{1.12}\text{Sb}_{0.88}$. b) Comparison of the RT magnetic hardness parameter κ with other hard magnets. The light gray plane marks the threshold $\kappa = 1$. c) Unit cell of tetragonal Heusler compound Rh_2CoSb , whose magnetocrystalline anisotropy surface shows easy-axis anisotropy along c .

$\text{Rh}_2\text{Mn}_{1.12}\text{Sn}_{0.88}$, Rh_2FeSn , and Rh_2CoSn and Rh_2CoSb ^[15] with 3d transition elements Mn, Fe, and Co, crystallize in a tetragonal structure with space group $I4/mmm$ ($D0_{22}$ structure). The 4d element Rh provides a strong spin–orbit interaction that contributes to the magnetocrystalline anisotropy in the tetragonal lattice.^[23]

Both X-ray diffraction (XRD) and transmission electron microscopy (TEM) experiments show that Rh_2CoSb has a well-ordered tetragonal $D0_{22}$ structure with $a = 4.0393$ (6) Å and $c = 7.1052$ (7) Å. Here, the 4d (0 0 $\frac{1}{4}$) site is occupied by Rh, 2b (0 0 $\frac{1}{2}$) by Co, and 2a (0 0 0) by Sb as shown in Figure 1c. The tetragonal distortion $c/\sqrt{2}a = 1.2436(3)$ agrees with the published value,^[15] being the largest among all reported Rh-based magnetic Heusler compounds. A sketch of the easy-axis energy surface is included in Figure 1c.

Unlike many Mn-based Heusler compounds, which are often cubic at high temperature and may undergo a martensitic phase transition to become tetragonal, Rh_2CoSb does not have a first-order transition at high temperature and remains in the tetragonal phase at all temperatures up to the melting point of 1482 K. A differential scanning calorimeter (DSC) measurement showing only the melting transition is presented in the Supporting Information. Since the phase melts congruently, single crystals can be grown by the Bridgeman method. They were cut along the c and a axes for further measurements and fully characterized by XRD, wavelength-dispersive X-ray spectroscopy (WDX), and TEM in the Supporting Information. WDX establishes a homogenous composition of $\text{Rh}_{50.3}\text{Co}_{25.6}\text{Sb}_{24.1}$

(see the Supporting Information). Errors in composition range from 0.1% to 0.2%.

Magnetic properties were measured along the c and a axes of single crystals as illustrated in Figure 2. A magneto-optical Kerr microscopy study^[24] shows surface domains with a two-phase branched pattern of higher generation on the (001) surface, which is commonly observed in uniaxial magnets. At 2 K, the magnetization along c saturates easily, at $37.5 \text{ A m}^2 \text{ kg}^{-1}$. Taking the density of $11\,030 \text{ kg m}^{-3}$ into consideration, the saturation magnetization $\mu_0 M_s$ is 0.52 T, which is similar to that of pure nickel. It corresponds to a moment of $2.6 \mu_B$ per Rh_2CoSb formula unit. The noninteger magnetic moment per unit cell indicates that Rh_2CoSb is not a half-metal. A field of $\mu_0 H_a$ of 175 T is required to saturate the sample along the a axis, where H_a is the anisotropy field. The magnetocrystalline anisotropy constant $K_1 = \frac{1}{2} \mu_0 H_a M_s$ is 3.6 MJ m^{-3} , which is larger than for any other rare-earth-free compound except for CoPt and FePt. Its relatively small M_s makes κ larger than for these materials and coercivity may exceed that of FePt.^[3] Both $\mu_0 M_s$ and K_1 decrease with increasing temperature, as shown in Figure 2b, but at room temperature they are still 0.44 T and 2.2 MJ m^{-3} , respectively. Big Barkhausen jumps observed during c axis demagnetization, together with a high initial susceptibility after thermal demagnetization indicate that single-crystal Rh_2CoSb is a nucleation type magnet.^[25,26] Detailed measurements of the magnetization along c and a at different temperatures are reported in the Supporting Information.

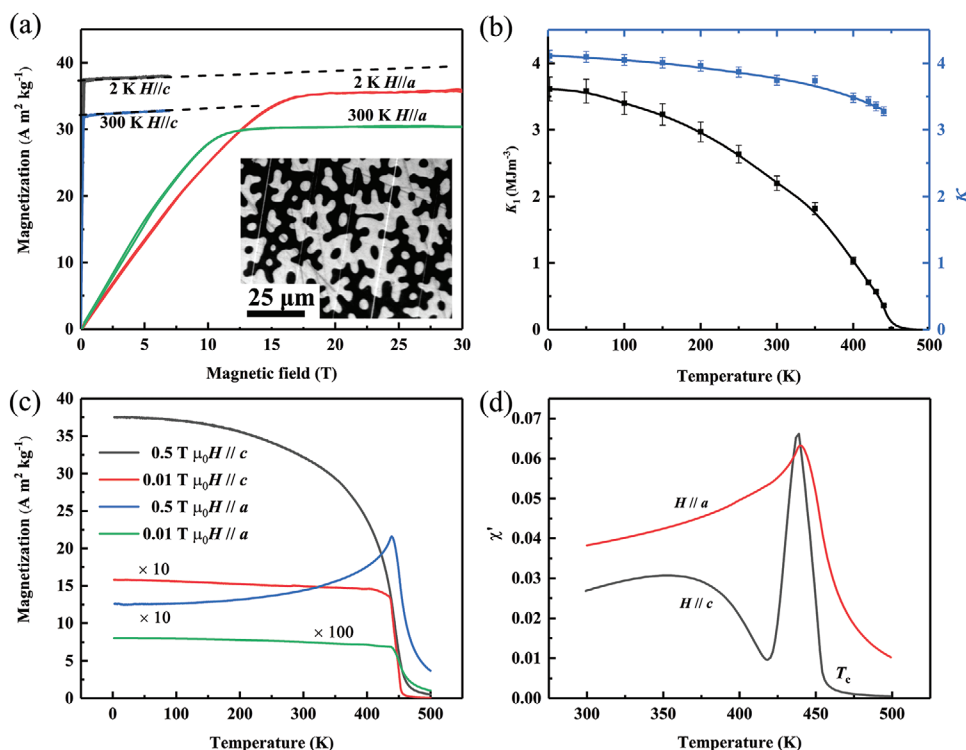


Figure 2. Magnetic properties of Rh_2CoSb . a) Magnetization curves at 2 and 300 K with the field along the a or c axes. The inset shows a pattern of branched domains at the surface perpendicular to the c axis, typical of a strong uniaxial ferromagnet. b) Magnetocrystalline anisotropy calculated from magnetization curves at different temperatures. The blue line shows the magnetic hardness parameter κ at different temperatures. c) Magnetization at different temperatures with the field along a or c axes. For better visibility, some values are enlarged by a factor of 10 or 100, depending on the field direction and the value of H . d) AC-susceptibility near T_c , showing a typical Hopkinson peak, due to the rapid increase of anisotropy just below T_c .

The Curie temperature is deduced to be 450 K from the temperature scans of magnetization in a 10 mT field. The M – T curve measured along the hard axis in a magnetic field of 0.5 T exhibits a sharp peak at 440 K, indicating a rapid built-up of anisotropy just below T_c . The slope dK_1/dT is 20 kJ m⁻³ K⁻¹ (twice as large as for FePt^[27]). The ac-susceptibility χ near T_c is shown in Figure 2d. It exhibits a typical Hopkinson peak along the c axis.^[15,28] Since $\chi \propto M_s^2/K_1$, during cooling, the rates of increase of M_s and K_1 vary differently at temperatures near T_c , giving a trough in ac susceptibility below the Hopkinson peak. There is nothing unusual in our M – T and M – H measurements at this temperature.

We compare in Figure 1b the room-temperature magnetic hardness parameter of Rh₂CoSb with other materials that exhibit $\mu_0 M_s > 0.4$ T, which is taken as a threshold necessary for useful stray fields. κ is a practical figure of merit for hard magnetic materials that must be greater than 1 if the material is to resist self-demagnetization when fabricated into any desired shape.^[4] Rh₂CoSb has $\kappa = 4.1$ at 2 K and 3.7 at room temperature, which is more than any other rare-earth-free magnet. Only SmCo₅ has a larger value.

All the indications are that Rh₂CoSb has the potential to be a good hard magnet with strong uniaxial anisotropy. There is no structural transition, avoiding the problems of decomposition (MnBi decomposes at 628 K) or twinning (like many nearly cubic rare-earth-free magnets such as MnGa, MnAl, FePt, and CoPt^[29]). Unlike many rare-earth magnets, the sample is stable in air and its magnetic properties have been found to remain unchanged for a year.

Thanks to the strong K_1 at 300 K, Rh₂CoSb promises a significant reduction in thermally stable grain size from diameter $D = 7$ – 9 nm in today's perpendicular Co–Cr–Pt media down to $D = 4$ – 5 nm in future Rh₂CoSb media, resulting in a potential storage density of more than 10 Terabit in.⁻² (for $D = 5$ nm with half the area occupied by hard grains). Detailed calculation can be found in the Supporting Information. HAMR media with grain diameters of only a few nm are hard to fabricate because the grains must be exchange decoupled by an intergranular material. Powder XRD data revealed the presence of a few percent of a RhSb secondary phase in our polycrystalline samples. Nonmagnetic RhSb appears at the grain boundaries, pinning the domains and creating hysteresis. It is a candidate for separating the nanocrystal grains in Rh₂CoSb thin-film media.

Transport properties of Rh₂CoSb are presented in Figure 3. The resistivity is very anisotropic. With increasing temperature, the a -axis resistivity increases monotonically from 53 $\mu\Omega$ cm at 2 K to 192 $\mu\Omega$ cm at T_c , after which the resistivity, dominated by spin disorder scattering, tends to saturate.^[30] The c -axis resistivity is less than half as large at 2 K, 21 $\mu\Omega$ cm, but it increases with temperature and shows a similar trend to the a -axis resistivity. The difference is due to intrinsic mobility and extrinsic domain wall scattering perpendicular to the c axis.^[31] Magnetoresistance and Hall measurements are also very anisotropic (see the Supporting Information).

The Seebeck coefficient is about -10 W K⁻¹ m⁻¹ at 300 K along both axes (c and a) with an error of $\pm 10\%$. The opposite signs of the Hall effect (positive) and Seebeck coefficient (negative) indicate the co-existence of both light holes and heavy electrons at the Fermi energy.^[32] Detailed data are presented in the Supporting Information. The spin polarization P of the electrons at the Fermi level was deduced from a point contact Andreev reflection measurement at 2 K (see the Supporting Information). The measured value of P is 13% and agrees well with the calculated spin polarization of the density of states at the Fermi energy (see the Supporting Information). The transport polarization will be different due to different effective masses of minority and majority electrons.^[33]

The measured thermal transport properties in Figure 3b,c along the c and a axes are also highly anisotropic. The total thermal conductivity along c is about twice as large as along a , and it is mainly explained by the carrier contribution, following the Wiedemann–Franz law.^[34] The remaining, almost isotropic, part is dominated by the phonon contribution. The slight upturn of the thermal conductivity at temperatures above 200 K may be due to uncertainty in the radiative heat loss, which is estimated to be about $\pm 10\%$. In addition, magnons or electron–magnon interactions might influence the thermal conductivity. The limiting Lorenz number generally depends a little on temperature.^[34] The anisotropy reflects the anisotropic electronic structure, which is the origin of the giant magnetocrystalline anisotropy. The c -axis thermal conductivity of 20 W m⁻¹ K⁻¹ at room temperature is roughly twice that of unsegregated L1₀ FePt (11–13 W m⁻¹ K⁻¹^[35,36]), or A1 FePt (9 W m⁻¹ K⁻¹^[36]). The anisotropic transport properties, including magnetoresistance, anomalous Hall effect, and Seebeck effect, result from the anisotropic electronic structure that leads to an anisotropic mobility of the charge carriers.

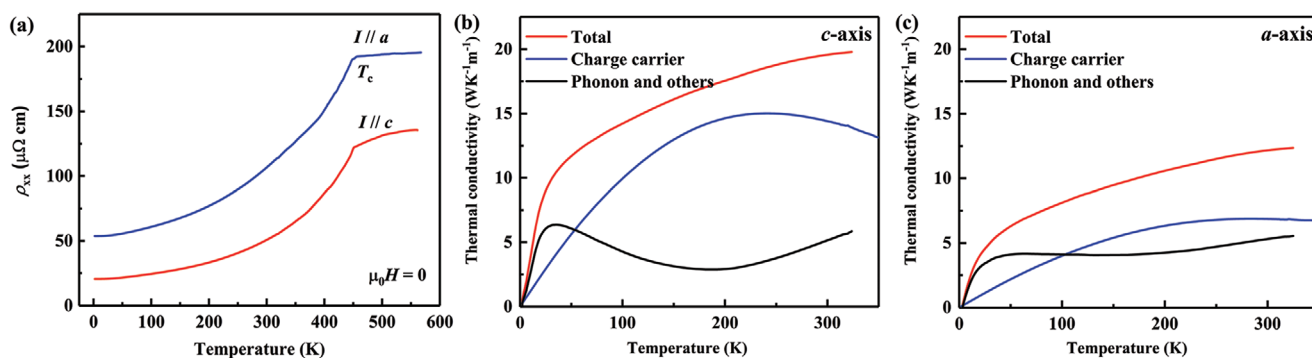


Figure 3. Transport properties of Rh₂CoSb. a) Longitudinal resistivity along the c (red curve) and the a axis (blue curve). b,c) Thermal conductivity along the c and a axes and the charge carrier contribution (estimated from the Wiedemann–Franz law as LT/ρ_{xx} , where $L = 2.44$ W Ω K⁻² is the Lorenz number). The remaining part is mainly the phonon contribution.

Little information is available about the magnetism of hard magnetic 3d–4d intermetallic compounds, other than FePd, which has the tetragonal $L1_0$ structure with $K_1 = 1.8 \text{ MJ m}^{-3}$, and YCo_5 which has the hexagonal CaCu_5 structure^[5] with $K_1 = 6.5 \text{ MJ m}^{-3}$. A number of ternary, tetragonal Rh-based intermetallics are known to order ferromagnetically with a Curie point above room temperature.^[15] Only one atom out of four in the Rh_2CoSb formula is cobalt, but the high T_c of 450 K indicates a strong exchange interaction. We see from our ab initio calculations (Supporting Information) that Rh is clearly in a spin-polarized state, and that it contributes to the ferromagnetism. The measured magnetic moment per formula of $2.6 \mu_B$ is much higher than the ordinary $\approx 1.6 \mu_B$ moment of Co in the elemental state or in metallic alloys with other 3d elements. The difference should be attributed, at least partially, to Rh, or else to enhanced Co spin and orbital moments, as there is no magnetic contribution from Sb.

We also prepared polycrystalline Rh_2FeSb with the same crystal structure, which exhibits easy-plane magnetization. At 300 K under 7 T, the incompletely saturated moment reaches $3.8 \mu_B$ per formula, far greater than the $2.2 \mu_B$ of metallic iron. The Curie temperature of 510 K is even higher than that of Rh_2CoSb , which is in contrast with other isostructural Fe and Co intermetallics. A detailed comparison of the spin and orbital contributions for Rh_2FeSb and Rh_2CoSb deduced from ab initio calculations is provided in the Supporting Information. All the evidence suggests that Rh plays an important role in the ferromagnetism of these ternary compounds. In fact, it has already been shown to carry an induced moment in binary Fe–Rh and Co–Rh alloys that is roughly one-third of the 3d moment.^[37,38]

To reveal the site-specific magnetic moments of Rh and Co, X-ray magnetic circular dichroism (XMCD) measurements were performed at the $L_{2,3}$ edges of Co and Rh, respectively. The spin and orbital moments of each element^[39–41] are determined from XMCD using sum rule analysis.^[42,43] The same number of 78 electrons in the valence d shell is assumed for both Co and Rh. This value was found in fully relativistic ab initio calculations.^[44] The measured XMCD spectra are shown in Figure 4. The XMCD signal has the same sign in the spectra obtained at the Co and Rh $L_{2,3}$ edges, which proves that the coupling between Co and Rh is ferromagnetic.

The XMCD signal at the L_3 edge for Co is considerably larger than that at the L_2 edge, which indicates a sizeable orbital contribution. Sum rule analysis reveals that spin and orbital moments for Co are $1.53 \pm 0.15 \mu_B$ and $0.42 \pm 0.04 \mu_B$, respectively. The orbital moment of Co in Rh_2CoSb far surpasses that of elemental Co, where the value is $0.15 \mu_B$.^[45] Therefore, the orbital moment of Co makes a sizeable contribution to the overall magnetization of $1.95 \pm 0.19 \mu_B$. The presence of a large orbital moment is also evident in Figure 2a from the $0.2 \mu_B$ difference of saturation magnetization between the c and a directions.

The spin and orbital moments of Rh obtained from the sum rule analysis are $0.28 \pm 0.03 \mu_B$ and $0.020 \pm 0.002 \mu_B$, respectively, resulting in a total moment of $0.30 \pm 0.03 \mu_B$. These values account for the reduced photon polarization at high energies. Using these moments, together with those of Co, the total magnetic moment of Rh_2CoSb should amount to $2.55 \pm 0.22 \mu_B$, which is in good agreement with the magnetic measurement of $2.6 \mu_B$.

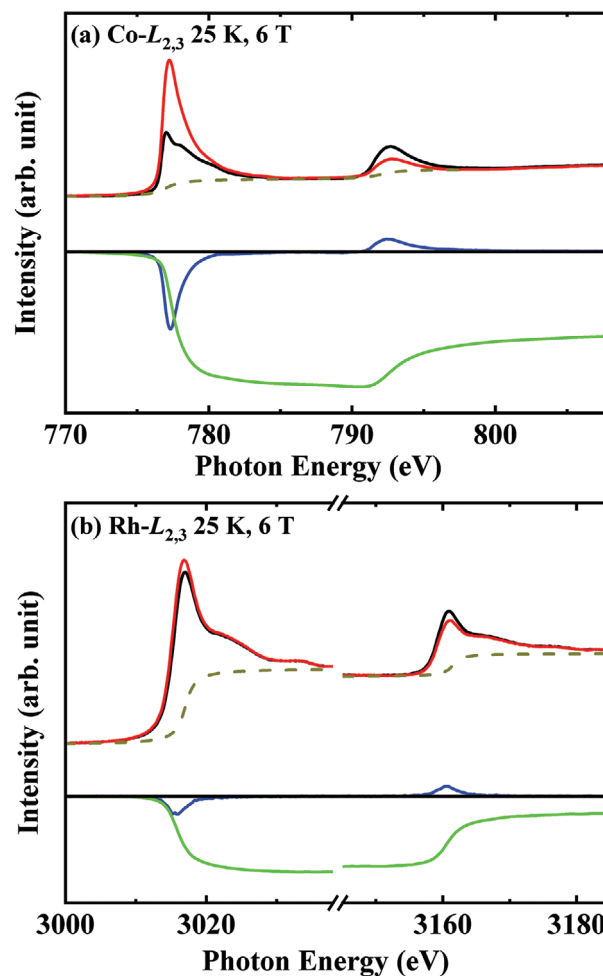


Figure 4. XAS and XMCD spectra of Rh_2CoSb . a) Co $L_{2,3}$ and b) Rh $L_{2,3}$ XAS and XMCD spectra. Spectra were taken at 25 K temperature and 6 T induction field. The photon helicity is oriented parallel (μ^{\parallel}) in black solid line or antiparallel ($\mu^{\text{anti-}\parallel}$) to the magnetic field. The background is shown in the black dash line with edge jumps.

The Co atoms have a substantial orbital magnetic moment in Rh_2CoSb , both from experiments and ab initio calculations. The orbital moment was 27% of the spin moment, compared to 5% in elemental α -Co (hcp) and 3% for Fe in calculations of the sister compound Rh_2FeSb . The larger orbital moment for cobalt reflects the hybridization of Co 3d states with 4d states of Rh, which has a stronger spin–orbit interaction than Co.

In many Heusler compounds, the martensitic transition from a cubic to a tetragonal structure is explained by a band Jahn–Teller effect^[23] that results in a splitting of energy levels by a modification of their width. We also calculated Rh_2CoSb in the higher energy cubic $L2_1$ structure, but saw no sign of Jahn–Teller-type splitting in the electronic structure. The formation enthalpies for our compound in the tetragonal $I4/mmm$ (space group 139), inverse tetragonal $I4m2$ (space group 119) and cubic $L2_1$ (space group 225) structures are -753 , -325 , and -221 meV , respectively. The energy difference between the cubic and tetragonal structures is 532 meV, significantly more than in other Rh-based Heusler compounds. Thus, the hypothetical

Table 1. Comparison of Rh₂CoSb with L1₀ FePt for HAMR at room temperature. The properties for Rh₂CoSb at 2 K is shown in brackets.

Materials	Crystal structure	K_1 [MJ m ⁻³]	$\mu_0 M_s$ [T]	$\mu_0 H_a$ [T]	κ	T_c [K]	$T_{\text{cub-tet}}$	Thermal stability	Thermal conductivity [W m ⁻¹ K ⁻¹]	Writing speed
Rh ₂ CoSb	<i>I4/mmm</i>	2.2 (3.6)	0.44 (0.52)	12 (17)	3.7 (4.1)	450	> melting point	Stable	20 in <i>c</i> axis 12 in <i>a</i> axis	Fast
L1 ₀ FePt	<i>P4/mmm</i>	6.6	1.43	11	2	750	1573 K	Transition to A1 FePt	11	Slow

cubic to tetragonal phase transition temperature ($T_{\text{cub-tet}}$) should be above the melting point. Among the reported Rh₂CoZ Heusler compounds, only Rh₂CoSb and Rh₂CoSn are tetragonal at room temperature; the others are cubic. However, Rh₂CoSn has a martensitic transition at around 600 K with a cubic structure at higher temperature.^[23] By avoiding any such transition, Rh₂CoSb is superior to other Rh₂CoZ alloys for HAMR media.

Our work will help to design new rare-earth-free materials with strong uniaxial magnetocrystalline anisotropy, for which we need:

- 1) a low-symmetry crystal structure (tetragonal or hexagonal);
- 2) heavy atoms with a large spin-orbit interaction (4d, 5d, or 5f elements);
- 3) another possible element with the right electronegativity to help stabilize the structure and help produce an advantageous electronic structure.

The magnetic moments of heavy non-rare-earth elements are small at best. Therefore, the design rule for rare-earth-free metallic magnets is to pair a 3d metal (Mn, Fe, Co) that can provide most of the magnetization with a heavy atom that supplies a large spin-orbit interaction. Rh, Ir, Pd, and Pt are all possible choices, since they are in the same group as Co or Ni and they may exhibit a significant induced magnetization.^[37,38,46] In fact, Pd is already ferromagnetic with $T_c = 17$ K if lightly doped with 0.5% of Co^[47] and when it is alloyed with 50% Co, it has the highest T_c among the binary compounds CoRh (550 K), CoIr (40 K), CoPd (950 K), and CoPt (840 K).^[48,49] Our study outlines the design principles for new rare-earth-free hard magnets, but it is unrealistic to imagine that Rh-based alloys will ever be used as bulk functional materials, in view of its high cost. This is much less important in functional thin films, because the quantities used are tiny. Strong perpendicular anisotropy is of increasing importance in spintronics and especially in HAMR, where thermal conductivity is also an important consideration.

Faleev et al.^[16] reported the preparation of Rh₂CoSb films by sputtering or ion-beam deposition between 373 and 873 K. A large perpendicular anisotropy was observed. Disorder is common in sputtered films. Our experiments indicate that the Rh is well ordered, but there might be some disorder between Co and Sb atoms. From ab initio calculations, the most stable crystal structure for both ordered and disordered phases is the tetragonal D0₂₂ structure and the lattice constant is very similar. The total magnetic moment in the fully Co-Sb disordered state is about 20% larger compared to the completely ordered state. The orbital moment is nearly constant and independent of the degree of disorder, so the increase of the total moment is attributed to the spin moment.

We compare Rh₂CoSb with L1₀ FePt^[5] for HAMR in **Table 1**. The magnetic properties for Rh₂CoSb at 2 K are shown with brackets, while those at 300 K are shown without brackets. The magnetic properties for L1₀ FePt do not vary much between 2 and 300 K. The writing speed is limited by the cooling time when the total heat produced by the laser transfers to the substrate. Since Rh₂CoSb has a much lower Curie point and higher thermal conductivity, its writing speed will be roughly 6.8 times faster than L1₀ FePt (see the Supporting Information).

In summary, Rh₂CoSb is a uniaxial ferromagnet with a remarkable magnetocrystalline anisotropy of 3.6 MJ m⁻³, due to a large unquenched orbital moment of 0.42 μ_B on Co that arises from hybridization with the surrounding Rh, where spin-orbit coupling is strong. The magnetic hardness parameter of $\kappa = 3.7$ at room temperature is the highest observed so far in any rare-earth-free magnet. The relatively low Curie point of $T_c = 450$ K leads to a large temperature dependence of K_1 from a high base at room temperature, which is an asset for data writing. The anisotropic thermal conductivity, especially its large *c* axis value of 20 W m⁻¹ K⁻¹, which is much larger than that of the current FePt HAMR material, is important for cooling, and could lead to a 6.8 times faster writing speed than FePt. Unlike FePt with its order/disorder phase transition, Rh₂CoSb is a stable phase without any structural transition below the melting point and its properties are stable in air. All these features commend Rh₂CoSb as a candidate for HAMR media with a recording density of more than 10 Tb in.⁻² and high writing speed.

Experimental Section

Single-Crystal Growth: The single crystals of Rh₂CoSb were grown by the Bridgeman method. First, the high purity (>99.99%) elements Rh, Co, and Sb were cut into small pieces and arc-melted together to prepare polycrystalline samples. The initial atomic ratio of Rh, Co, and Sb was 2:1:1.03. Additional Sb was added to compensate for its high vapor pressure. From powder XRD data, there were always a few percent of a RhSb secondary phase in the polycrystalline samples. Hence the polycrystalline materials were heated up to 1600 K (above the melting point of RhSb at 1583 K) for 3 days to achieve a homogenous liquid before beginning the single-crystal growth, which took about 5 days during cool down to 1273 K. The composition of the crystals was checked by wavelength-dispersive X-ray spectroscopy that showed a homogenous composition of Rh_{50.3}Co_{25.6}Sb_{24.1}. The crystals were characterized by powder XRD as single-phase with a tetragonal structure. The orientation of the single crystals was confirmed by the Laue method.

Magnetization Measurements: These were conducted on single crystals with the magnetic field applied along either the *a* or *c* axis using a vibrating sample magnetometer (MPMS 3, Quantum Design). The sample size was 3.80 × 0.78 × 1.30 mm³. For measurement with the field along the *a* axis, the sample was carefully immobilized with glue in view of the strong torque. High-field magnetization measurements were performed in the Dresden High Magnetic Field Laboratory using a pulsed magnet.

Magneto-Optical Kerr Microscopy: Domain images were performed by using the polar Kerr effect in a wide-field magneto-optical Kerr microscope at room temperature on a polished (100) surface of a 1 mm thick single crystal. A detailed description of the method can be found elsewhere.^[50]

Electrical Transport Measurements: The longitudinal and Hall resistivities were measured on a Quantum Design PPMS 9 using the low-frequency alternating current (ACT) option for data below 320 K. The longitudinal resistivity was measured with standard four-probe method, while for the Hall resistivity measurements, the five-probe method was used with a balance protection meter to eliminate possible magnetoresistance signals. Longitudinal resistivity measurement above 320 K was measured on a home-made device using a four-probe method and careful calibration. The accuracy of resistivity measurement was $\pm 5\%$.

Thermal Transport Measurements: The thermal conductivity and Seebeck thermopower were measured adiabatically in the Quantum Design PPMS using thermal transport option. The uncertainty of the radiative heat losses at high temperature and the uncertainty of the geometry were estimated as $\pm 10\%$.

Andreev Reflection Measurements: Measurements were performed on a polished (001) crystal surface in a flow of helium vapor, using a mechanically sharpened Nb tip in the absence of an external magnetic field. Data were analyzed using the modified Blonder–Tinkham–Klapwijk (BTK) model, as detailed elsewhere.^[51] The best fit to spectrum was obtained with barrier parameter Z of ≈ 0.35 , an electron temperature of 2 K, and a spin polarization of 13%.

XMCD Measurements: XMCD was measured at the beamline BL29 (BOREAS) of the synchrotron ALBA in Barcelona (Spain). XMCD spectra at the $L_{2,3}$ absorption edges of Co and Rh were taken at a temperature of 25 K in a vacuum chamber with a pressure of 10^{-9} mbar. The X-ray absorption spectra (XAS) were measured using circular polarized light with photon helicity parallel (μ^+) or antiparallel (μ^-) to the fixed magnetic field in the sequence $\mu^+\mu^-\mu^+\mu^-\mu^+\mu^-\mu^+\mu^-$ to disentangle the XMCD. An induction field of 6 T was applied along the c axis. The polarization delivered by the Apple II-type elliptical undulator was close to 100% for the Co $L_{2,3}$ edges and 70% for the Rh $L_{2,3}$ edges. The spectra were recorded using the total yield mode.

Supporting Information

Supporting Information is available from the Wiley Online Library or from the author.

Acknowledgements

This work was financially supported by the European Research Council Advanced Grant (no. 742068) “TOPMAT,” the European Union’s Horizon 2020 research and innovation programme (no. 824123) “SKYTOP,” the European Union’s Horizon 2020 research and innovation programme (no. 766566) “ASPIN,” the Deutsche Forschungsgemeinschaft (Project-ID 258499086) “SFB 1143,” the Deutsche Forschungsgemeinschaft (Project-ID FE 633/30-1) “SPP Skyrmions,” the DFG through the Würzburg-Dresden Cluster of Excellence on Complexity and Topology in Quantum Matter ct.qmat (EXC 2147, Project-ID 39085490), and the DFG through SFB 1143. The authors acknowledge the support of the High Magnetic Field Laboratory Dresden (HLD) at HZDR, members of the European Magnetic Field Laboratory (EMFL).

Open access funding enabled and organized by Projekt DEAL.

Conflict of Interest

The authors declare no conflict of interest.

Author Contributions

Single crystals were grown by Y.H. and K.M. The characterization of the crystal, magnetic, and transport measurement were performed by Y.H. with the help of C.F., Y.P., J.K., A.J., Y.S., W.S., P.S., H.B., R.S., and S.S.P.P. XMCD was measured by X.W., Z.H., S.A., J.H., M.V., and L.H.T. First-principle calculations were carried out by G.H.F. All the authors discussed the results. The paper was written by Y.H., J.M.D.C., and G.H.F. with feedback from all the authors. The project was supervised by C.F.

Keywords

4d magnetism, magnetic hardness parameter, magnetic recording, magnetocrystalline anisotropy, tetragonal Heusler alloys

Received: June 25, 2020

Revised: September 2, 2020

Published online: October 7, 2020

- [1] C. Chappert, A. Fert, F. N. V. Dau, *Nat. Mater.* **2007**, 6, 813.
- [2] M. T. Kief, R. H. Victora, *MRS Bull.* **2018**, 43, 87.
- [3] D. Weller, G. Parker, O. Mosendz, A. Lyberatos, D. Mitin, N. Y. Safonova, M. Albrecht, *J. Vac. Sci. Technol., B: Microelectron. Nanometer Struct.–Process., Meas., Phenom.* **2016**, 34, 060801.
- [4] R. Skomski, J. M. D. Coey, *Scr. Mater.* **2016**, 112, 3.
- [5] J. M. D. Coey, *Magnetism and Magnetic Materials*, Cambridge University Press, Cambridge, UK **2010**, Ch. 4 and 8.
- [6] S. I. Iwasaki, K. Ouchi, *IEEE Trans. Magn.* **1978**, 14, 849.
- [7] L. Pan, D. B. Bogy, *Nat. Photonics* **2009**, 3, 189.
- [8] J. M. Hu, L. Q. Chen, C. W. Nan, *Adv. Mater.* **2016**, 28, 15.
- [9] W. A. Challener, C. Peng, A. V. Itagi, D. Karns, W. Peng, Y. Peng, X. Yang, X. Zhu, N. J. Gokemeijer, Y.-T. Hsia, G. Ju, R. E. Rottmayer, M. A. Seigler, E. C. Gage, *Nat. Photonics* **2009**, 3, 220.
- [10] A. V. Kimel, M. Li, *Nat. Rev. Mater.* **2019**, 4, 189.
- [11] D. Weller, O. Mosendz, G. Parker, S. Pisana, T. S. Santos, *Phys. Status Solidi A* **2013**, 210, 1245.
- [12] C.-B. Rong, D. Li, V. Nandwana, N. Poudyal, Y. Ding, Z. L. Wang, H. Zeng, J. P. Liu, *Adv. Mater.* **2006**, 18, 2984.
- [13] A. K. Nayak, A. K. Nayak, M. Nicklas, S. Chadov, P. Khuntia, C. Shekhar, A. Kalache, M. Baenitz, Y. Skourski, V. K. Guduru, A. Puri, U. Zeitler, J. M. D. Coey, C. Felser, *Nat. Mater.* **2015**, 14, 679.
- [14] H. Kurt, K. Rode, P. Stamenov, M. Venkatesan, Y.-C. Lau, E. Fonda, J. M. D. Coey, *Phys. Rev. Lett.* **2014**, 112, 027201.
- [15] S. K. Dhar, A. K. Grover, S. K. Malik, R. Vijayaraghavan, *Solid State Commun.* **1980**, 33, 545.
- [16] S. V. Faleev, Y. Ferrante, J. Jeong, M. G. Samant, B. Jones, S. S. P. Parkin, *Phys. Rev. Mater.* **2017**, 1, 024402.
- [17] T. Gasi, A. K. Nayak, J. Winterlik, V. Ksenofontov, P. Adler, M. Nicklas, C. Felser, *Appl. Phys. Lett.* **2013**, 102, 202402.
- [18] P. J. Brown, T. Kanomata, K. Neumann, K. U. Neumann, B. Ouladdiaf, A. Sheikh, K. R. A. Ziebeck, *J. Phys.: Condens. Matter* **2010**, 22, 506001.
- [19] B. Balke, G. H. Fecher, J. Winterlik, C. Felser, *Appl. Phys. Lett.* **2007**, 90, 152504.
- [20] A. K. Nayak, C. Shekhar, J. Winterlik, A. Gupta, C. Felser, *Appl. Phys. Lett.* **2012**, 100, 152404.
- [21] A. K. Nayak, M. Nicklas, S. Chadov, C. Shekhar, Y. Skourski, J. Winterlik, C. Felser, *Phys. Rev. Lett.* **2013**, 110, 127204.
- [22] O. Meshcheriakova, S. Chadov, A. K. Nayak, U. K. Röbber, J. Kübler, G. André, A. A. Tsirlin, J. Kiss, S. Hausdorf, A. Kalache, W. Schnelle, M. Nicklas, C. Felser, *Phys. Rev. Lett.* **2014**, 113, 087203.

- [23] J. C. Suits, *Solid State Commun.* **1976**, *18*, 423.
- [24] A. Hubert, R. Schäfer, *Magnetic Domains*, Springer, Berlin, Germany **1998**, pp. 314–379.
- [25] Y. Otani, J. M. D. Coey, *J. Appl. Phys.* **1990**, *67*, 4619.
- [26] T. Nishioka, G. Motoyama, N. K. Sato, *J. Magn. Magn. Mater.* **2004**, *272–276*, E151.
- [27] S. Okamoto, N. Kikuchi, O. Kitakami, T. Miyazaki, Y. Shimada, K. Fukamichi, *Phys. Rev. B* **2002**, *66*, 024413.
- [28] M. Balanda, *Acta Phys. Pol., A* **2013**, *124*, 964.
- [29] J. Cui, M. Kramer, L. Zhou, F. Liu, A. Gabay, G. Hadjipanayis, B. Balasubramanian, D. Sellmyer, *Acta Mater.* **2018**, *158*, 118.
- [30] C. Hass, *Phys. Rev.* **1968**, *168*, 531.
- [31] D. Elefant, R. Schäfer, *Phys. Rev. B* **2010**, *82*, 134438.
- [32] J. Dijkstra, H. H. Weitering, C. F. Van Bruggen, C. Haas, R. A. De Groot, *J. Phys.: Condens. Matter* **1989**, *1*, 9141.
- [33] G. H. Fecher, S. Chadov, C. Felser, in *Spintronics from Materials to Devices* (Eds: C. Felser, G. H. Fecher), Springer, Dordrecht, The Netherlands **2013**, pp. 115–165.
- [34] J. M. Ziman, *Electrons and Phonons*, Oxford University Press, Oxford **1960**.
- [35] A. Chernyshov, D. Treves, T. Le, F. Zong, A. Ajan, R. Acharya, *J. Appl. Phys.* **2014**, *115*, 17B735.
- [36] A. Giri, S. H. Wee, S. Jain, O. Hellwig, P. E. Hopkins, *Sci. Rep.* **2016**, *6*, 32077.
- [37] G. R. Harp, S. S. P. Parkin, W. L. O'Brien, B. P. Tonner, *Phys. Rev. B* **1995**, *51*, 12037.
- [38] G. R. Harp, S. S. P. Parkin, W. L. O'Brien, B. P. Tonner, *J. Appl. Phys.* **1994**, *76*, 6471.
- [39] S. Agrestini, Z. Hu, C.-Y. Kuo, M. W. Haverkort, K.-T. Ko, N. Hollmann, Q. Liu, E. Pellegrin, M. Valvidares, J. Herrero-Martin, P. Gargiani, P. Gegenwart, M. Schneider, S. Esser, A. Tanaka, A. C. Komarek, L. H. Tjeng, *Phys. Rev. B* **2015**, *91*, 075127.
- [40] S. Das, A. D. Rata, I. V. Maznichenko, S. Agrestini, E. Pippel, N. Gauquelin, J. Verbeeck, K. Chen, S. M. Valvidares, H. Babu Vasili, J. Herrero-Martin, E. Pellegrin, K. Nenkov, A. Herklotz, A. Ernst, I. Mertig, Z. Hu, K. Dörr, *Phys. Rev. B* **2019**, *99*, 024416.
- [41] N. Hollmann, S. Agrestini, Z. Hu, Z. He, M. Schmidt, C.-Y. Kuo, M. Rotter, A. A. Nugroho, V. Sessi, A. Tanaka, N. B. Brookes, L. H. Tjeng, *Phys. Rev. B* **2014**, *89*, 201101(R).
- [42] B. T. Thole, P. Carra, F. Sette, G. van der Laan, *Phys. Rev. Lett.* **1992**, *68*, 1943.
- [43] P. B. Carra, T. Thole, M. Altarelli, X. Wang, *Phys. Rev. Lett.* **1993**, *70*, 694.
- [44] G. H. Fecher, Y. He, C. Felser, arXiv:2009.00920, **2020**.
- [45] C. T. Chen, Y. U. Idzerda, H.-J. Lin, N. V. Smith, G. Meigs, E. Chaban, G. H. Ho, E. Pellegrin, F. Sette, *Phys. Rev. Lett.* **1995**, *75*, 152.
- [46] V. V. Krishnamurthy, D. J. Singh, N. Kawamura, M. Suzuki, T. Ishikawa, *Phys. Rev. B* **2006**, *74*, 064411.
- [47] A. Pilipowicz, H. Claus, *Phys. Rev. B* **1987**, *36*, 773.
- [48] H. Masumoto, K. Watanabe, K. Inagawa, *J. Jpn. Inst. Met.* **1976**, *17*, 592.
- [49] B. Predel, H. Landolt, R. Börnstein, P. equilibria, *Crystallographic and Thermodynamic Data of Binary Alloys*, Vol. 5, Springer, Heidelberg/Berlin, Germany **1991**.
- [50] I. V. Soldatov, R. Schäfer, *Rev. Sci. Instrum.* **2017**, *88*, 073701.
- [51] P. Stamenov, *J. Appl. Phys.* **2013**, *113*, 17C718.